AFRL-AFOSR-UK-TR-2013-0028

Examination of rotating spoke instability in a cross-field discharge

*** S. Mazouffre, L. Balika, J. Vaudolon**
**** R. Schneider, K. Matyash**
***** Y. Raitses, A. Diallo, Y. Shi**

*** CTRE Nat De La Recherche Scientifique, CNRS MOY800 CTRE Poitou Charente, 3, Ave Recherche Scientifique, Orleans 45000 France**
**** Ernst-Moritz-Arndt Universitat Greifswald, Greifswald, Germany**
***** Princeton Plasmas Physics Laboratory, Princeton, NJ 08540 USA**

EOARD Grant 12-2061

Report Date: July 2013

Final Report from 3 April 2012 to 30 June 2013

Distribution Statement A: Approved for public release distribution is unlimited.

Air Force Research Laboratory
Air Force Office of Scientific Research
European Office of Aerospace Research and Development
Unit 4515 Box 14, APO AE 09421

REPORT DOCUMENTATION PAGE

Form Approved OMB No. 0704-0188

Public reporting burden for this collection of information is estimated to average 1 hour per response, including the time for reviewing instructions, searching existing data sources, gathering and maintaining the data needed, and completing and reviewing the collection of information. Send comments regarding this burden estimate or any other aspect of this collection of information, including suggestions for reducing the burden, to Department of Defense, Washington Headquarters Services, Directorate for Information Operations and Reports (0704-0188), 1215 Jefferson Davis Highway, Suite 1204, Arlington, VA 22202-4302. Respondents should be aware that notwithstanding any other provision of law, no person shall be subject to any penalty for failing to comply with a collection of information if it does not display a currently valid OMB control number.
PLEASE DO NOT RETURN YOUR FORM TO THE ABOVE ADDRESS.

1. REPORT DATE *(DD-MM-YYYY)*	2. REPORT TYPE	3. DATES COVERED *(From – To)*
08 July 2013	Final Report	03 April 2012 – 30 June 2013

4. TITLE AND SUBTITLE

Examination of rotating spoke instability in a cross-field discharge

5a. CONTRACT NUMBER

FA8655-12-1-2061

5b. GRANT NUMBER

Grant 12-2061

5c. PROGRAM ELEMENT NUMBER

61102F

6. AUTHOR(S)

* S. Mazouffre, L. Balika, J. Vaudolon
** R. Schneider, K. Matyash
*** Y. Raitses, A. Diallo, Y. Shi

5d. PROJECT NUMBER

5d. TASK NUMBER

5e. WORK UNIT NUMBER

7. PERFORMING ORGANIZATION NAME(S) AND ADDRESS(ES)

* CTRE Nat De La Recherche Scientifique, CNRS MOY800 CTRE Poitou Charente, 3, Avenue Recherche Scientifique, Orleans 45000 France
** Ernst-Moritz-Arndt Universitat Greifswald, Greifswald, Germany
*** Princeton Plasmas Physics Laboratory, Princeton, NJ 08540

8. PERFORMING ORGANIZATION REPORT NUMBER

PE-R-04-2013

9. SPONSORING/MONITORING AGENCY NAME(S) AND ADDRESS(ES)

EOARD
Unit 4515
APO AE 09421-4515

10. SPONSOR/MONITOR'S ACRONYM(S)

AFRL/AFOSR/IOE (EOARD)

11. SPONSOR/MONITOR'S REPORT NUMBER(S)

AFRL-AFOSR-UK-TR-2013-0028

12. DISTRIBUTION/AVAILABILITY STATEMENT

Distribution A: Approved for public release; distribution is unlimited.

13. SUPPLEMENTARY NOTES

14. ABSTRACT

This joint experimental and theoretical project concerns rotating spoke phenomena in Hall thrusters. This is an international collaborative project between the CARE Institute (CNRS) in France, the High Performance Computing (HPC) group at the Ernst-Moritz-Arndt University in Germany, and the Princeton Plasmas Physics Laboratory in the USA. The main objective of this joint project was to obtain a better understanding of spoke physics through careful experiments and accompanying numerical simulations. The main task was the investigation of the influence of the spoke on the ion flow and its role in thrust and specific impulse generation as well as on the accelerating potential in a Cylindrical Hall Thruster (CHT). We also examine the rotating spoke instability formation and dynamics such as frequency, shape, and mode number and the electron transport arising from the spoke.

15. SUBJECT TERMS

EOARD, multiscale methods, mathematical modeling, stiff ODEs, turbulence

16. SECURITY CLASSIFICATION OF:			17. LIMITATION OF ABSTRACT	18, NUMBER OF PAGES	19a. NAME OF RESPONSIBLE PERSON
a. REPORT	b. ABSTRACT	c. THIS PAGE			Kevin Bollino
UNCLAS	UNCLAS	UNCLAS	SAR	37	19b. TELEPHONE NUMBER *(Include area code)* +44 (0)1895 616163

Examination of rotating spoke instability in a cross-field discharge

EOARD project

Grant FA8655-12-1-2061
June 2012 – June 2013

Final Report
PE-R-04-2013

8th of July, 2013.

ICARE – CNRS
S. Mazouffre (project leader), L. Balika, J. Vaudolon

EMAU
R. Schneider, K. Matyash

PPPL
Y. Raitses, A. Diallo, Y. Shi

PRINCETON PLASMA PHYSICS LABORATORY

ERNST MORITZ ARNDT UNIVERSITÄT GREIFSWALD

Wissen lockt. Seit 1456

Distribution A: Approved for public release; distribution is unlimited.

Distribution A: Approved for public release; distribution is unlimited.

Examination of rotating spoke instability in a cross-field discharge

Objective of the work

This joint experimental and theoretical project concerns rotating spoke phenomena in Hall thrusters. This is an international collaborative project between the **CARE Institute** (CNRS) in France, the **High Performance Computing (HPC) group** at the Ernst-Moritz-Arndt University in Germany, and the **Princeton Plasmas Physics Laboratory** in the USA.

The main objective of this joint project was to obtain a better understanding of spoke physics through careful experiments and accompanying numerical simulations. The main task was the investigation of the influence of the spoke on the ion flow and its role in thrust and specific impulse generation as well as on the accelerating potential in a Cylindrical Hall Thruster (CHT). We also planned to examine the rotating spoke instability formation and dynamics such as frequency, shape, and mode number and the electron transport arising from the spoke.

The project was originally divided into three successive phases, namely:

Phase 1: Time-averaged LIF study on the CHT at PPPL

Phase 2: Time-resolved LIF study on the CHT at ICARE

Phase 3: Time-resolved LIF study on a 2 kW HT at PPPL (Optional)

Distribution A: Approved for public release; distribution is unlimited.

Main achievements

A more detailed description of the main achievements is given in the next sections wherein an overview of works performed by the three teams is given.
Here only a brief summary is presented.

Program

Phase 1 and 2 of the project are achieved.

The ICARE team developed a pulse-counting technique for a low-power Cylindrical Hall thruster (CHT).
All experiments with the CHT have been carried out at the PPPL. It appeared the transfer of the device from the USA to France was an extremely complicated step which we decided to skip at the end.

In December, Dr. L. Balika from ICARE spent 3 weeks at PPPL to prepare the CHT and the LIF optical bench.
In March 2013, Dr. S. Mazouffre from ICARE spent 4 weeks at PPPL installing and testing the photon-counting technique and performing the first time-resolved measurements of ion velocity in a CHT with driven spoke instability.

Optional Phase 3 has not been performed.

This part concerns time-resolved LIF measurements in a high-power Hall thruster.
It was, however, optional in the original program.

Most significant accomplishments and results

- Demonstrated control of low-frequency discharge oscillations with injection of low amount of power in the discharge

    i) control and stabilization of rotating spoke instability in a CHT with a segmented anode

    ii) control and stabilization of the breathing mode in a low-power HT by way of modulation of the cathode electron stream

- Developed and applied Photon-counting technique with a 100 ns time resolution for time-resolved LIF measurements

    i) the technique was setup and successfully tested with a low-power permanent magnet Hall thruster at ICARE: measurements of the time-dependent Xe^+ ion axial VDF(t)

    ii) the technique was then transfer to PPPL for experiments with CHT.

- Developed optical bench, detection branch and counting device for time-resolving LIF at PPPL

- Conducted testing and qualification of time-averaged and time-resolved LIF (during visits of PPPL by L. Balika and S. Mazouffre of ICARE)

Distribution A: Approved for public release; distribution is unlimited.

- Conducted measurements of the time-dependent Xe^+ ion velocity distribution function (VDF) along the axis of the CHT
These measurements revealed:

i) low frequency oscillations of the ion density due to the rotating spoke

ii) the axial ion velocity component is not affected by spoke oscillations.

- Performed 3D PIC simulations of the rotating spoke in CHT at EMAU.
Comparison with results of PPPL-ICARE experiments. There is a qualitative agreement between predictions of PIC simulations and time-averaged and time-resolved LIF and probe measurements, including:

i) downstream shift of the electric potential drop in the presence of spoke oscillations

ii) asymmetry in the ion flow due to spoke

iii) the influence of the spoke on the axial ion velocity is minimal on the thruster axis

- Development and preliminary testing of a novel time-resolved LIF technique based on a heterodyne scheme (indirect approach as outcomes in Fourier space).
Foreseen advantages compared to direct approach: high signal-to-noise ratio, increased acquisition speed.
Practical applications can be found in the fields of EP and plasma physics in general.

Distribution A: Approved for public release; distribution is unlimited.

- List of publications and conferences related to the project

Journals

M. E. Griswold, C. L. Ellison, Y. Raitses, and N. J. Fisch, *Feedback control of an azimuthal oscillation in the E×B discharge of Hall thrusters*, Physics of Plasmas **19**, 053506 (2012).

W. Frias, A. I. Smolyakov, I. D. Kaganovich, and Y. Raitses, *Long wavelength gradient drift instability in Hall plasma devices*. *I. Fluid theory*, Physics of Plasmas **19**, 072112 (2012).

W. Frias, A. I. Smolyakov, I. D. Kaganovich, and Y. Raitses, *Long wavelength gradient drift instability in Hall plasma devices. II. Applications*, Phys. Plasmas **20**, 052108 (2013)

C. L. Ellison, K. Matyash, J. B. Parker, Y. Raitses, and N. J. Fisch, *Comment on Three-dimensional numerical investigation of electron transport with rotating spoke in a cylindrical anode layer Hall plasma accelerator*, Physics of Plasmas **20**, 014701 (2013).

J. Vaudolon, L. Balika, S. Mazouffre, *Photon counting technique applied to time-resolved laser-induced fuorescence measurements on a stabilized discharge*, accepted for publication in Rev. Sci. Instrum. (2013).

Conference proceedings

K. Matyash, R. Schneider, *Particle In Cell simulation of plasma thrusters*, IEEE Pulsed Power & Plasma Science Conference, San Francisco, California USA, June 16-21 2013.

K. Matyash, R. Schneider, S. Mazouffre, S. Tsikata, Y. Raitses, A. Diallo, *3D simulation of rotating spoke in a Hall thruster*, 33rd International Electric Propulsion Conference, Washington DC, USA, October 6 - 10, 2013.

Y. Raitses, M. Griswold, C. L. Ellison, J. Parker, and N. J. Fisch, *Studies of rotating spoke oscillations in cylindrical Hall thrusters*, AIAA paper 2012-4179, 48th Joint Propulsion Conference, Atlanta GA., August 2012

Y. Shi, A. Diallo, S. Mazouffre, and Y. Raitses, *Measurement of time-dependent ion velocity distribution function by laser induced fluorescence in a cylindrical Hall thruster with driven spoke*, Gaseous Electronics Conference, Princeton, NJ, October 2013.

Y. Shi, Y. Raitses, and A. Diallo, *Driving low frequency azimuthal modes in cylindrical Hall thrusters with segmented anode*, 33rd International Electric Propulsion Conference, Washington DC, USA, October 6 - 10, 2013.

A. Diallo, Y. Shi, Y. Raitses, S. Mazouffre, *Spoke-induced ion distribution velocity function perturbation in Hall thruster: An heterodyne approach with coupled wave excitation and laser-induced fluorescence*, 33rd International Electric Propulsion Conference, Washington DC, USA, October 6 - 10, 2013.

Distribution A: Approved for public release; distribution is unlimited.

Invited talks

Y. Raitses, C. L. Ellision, M. Griswald, J B Parker, K. Matyash and R. Schnedier, *Rotating spoke in Hall thrusters*, 39th IEEE International Conference on Plasma Science, Edinburg, UK , July 2012.

Y. Raitses, C. L. Ellision, M. Griswald, J B Parker, K. Matyash and R. Schnedier, *Rotating Spoke Phenomena in E cross B Discharges*, 65th Gaseous Electronics Conference, Austin, TX, October 2012.

Distribution A: Approved for public release; distribution is unlimited.

Photon counting technique for time-resolved laser-induced fluorescence measurements.

S. Mazouffre, J. Vaudolon, and L. Balika
CNRS – ICARE, Orléans, France

Background and goal

Low frequency oscillations associated with ionization are of great interest in Hall thruster operation as they usually carry a large portion of the spectrum energy content. They could also play a role in transport and cross field diffusion. Rotating plasma structures known as spokes as well as breathing mode oscillations in Hall thrusters are two examples of such an oscillation.
The investigation of the discharge properties naturally requires time-resolved measurements at the oscillation time scale. The electric field temporal evolution is a quantity of prime interest to describe ionization, acceleration and transport processes. We propose an optical method associated with a photon counting technique. The time-dependent Ion Velocity Distribution Function (IVDF) is accessible by means of Time-Resolved Laser-Induced Fluorescence (TR-LIF) on the ion population. In order to achieve time-resolved measurements, a specific set-up is necessary. First, the occurence frequency of fluorescence events must be below the maximum pulse counting rate of the detection system to stay within a linear regime. Second, the detection apparatus must be able to distinguish between LIF photons and background noise and to accumulate over several oscillation cycles. Third, a temporal resolution much below the oscillation time period is required. Finally, and most critical, reproducible measurement conditions imply temporal coherence of the oscillations. This is possible with a quasi-periodic behavior of the plasma parameters.
In this project, we examined a time-resolved photon counting technique combined with the control of the low frequency oscillations in a Hall thruster.

Hall thruster and oscillations control

For the experiments described here a 200 W input power class Hall thruster has been used [1]. The operating point was fixed to a discharge voltage of 200 V and an anode mass flow rate of 1.2 mg/s. Xenon was used as working gas for both the thruster and the hollow cathode. Alumina ceramics were used for the channel walls. The $2S_0$ geometry is used [1]. The thruster was operated in a 1.8 m in length and 0.8 m in diameter vacuum chamber evacuated by a cryogenic pump. The background pressure was kept at 7.10^{-5} mbar-N_2 during operation.

In order to achieve TR-LIF in a Hall thruster, the discharge needs to be maintained in a periodic oscillation regime. The active harmonic system presented here has two main advantages: first, the modulation signal can be used as a trigger signal. Second, the frequency content is the same at any time. Besides, our stabilizing technique warrants a constant frequency content during operation. In order to control the oscillations, a sinusoidal frequency-tunable potential is applied between a floating electrode in the vicinity of the cathode (referred to as the keeper) and the negative pole of the cathode. A schematic view is represented in Fig. 1. The modulation frequency cannot be choosen randomly but corresponds to a resonance of the system.

Fig. 2 shows the effect of the modulation system on the discharge current. First it is clear that the mean value of the discharge current remains unchanged, which is mandatory to keep the

Distribution A: Approved for public release; distribution is unlimited.

same thruster average behavior. Second, the discharge current amplitude is clearly higher with the modulation. Although it does not appear on a single screenshot, the ensemble averaging over mulitple acquisitions show a constant time-averaged amplitude. Third, the discharge current phase is constant, which ensures temporal coherence between each measurement pass. The current driven through the keeper is about 60 mA which corresponds to 5 W injected into a 200 W system. The possibility of modulating the discharge may subsequently be related to the ratio of the input power of the modulation amplifier to the power of the system to be modulated. A value of~10\% enables efficient control and does not disturb the thruster average behavior.

Time-resolved LIF technique

The LIF optical assembly is described in details in a review paper [2]. The optical transition at 834.72 nm that corresponds to long-lived metastable Xe^+ ions is probed by an amplified tunable single-mode external cavity laser diode. The wavelength is accurately measured by a high precision wave meter. A high finesse Fabry-Perot interferometer is used to check the laser stability and detect mode-hops. An anamorphosis filter circularizes the laser beam and maximize the transmission through the optical fiber. The laser beam propagates along the thruster axis and is aligned with the center of the discharge channel. The laser typical power density is 10 mW/m^2 within the measurement volume, which warrants a good signal-to-noise ratio and a limited saturation of the transition. A collection branch focuses the light onto a 200 μm core diameter optical fiber. The fluorescence light is focused onto the entrance slit of a 20 cm focal length monochromator that isolates the 541.9 nm line from the background ones. A photomultiplier tube serves as a light detector.

The photon counting technique has been applied in the past to diagnose oscillating and pulsed discharges [3]. However, so far it has never been used on a remotely stabilized discharge. Photons are detected by means of a high gain low dark noise PMT. The detection branch is schematized in Fig. 3. A fast amplifier and discriminator module is used to screen out the noise from the PMT. This has two advantages. First, the count rate is limited to avoid the pulse counter saturation. Second, any single event is converted into a TTL signal. In order to properly adjust the discriminator threshold, events are classified depending on their intensity. Each photon pulse can be distinguished from the background noise by appropriate setting of the discriminator threshold.
The pulse counting device is a multichannel scaler. The entire period of the oscillation can therefore be recorded. Moreover, any wave shape can be recorded with this technique. A modulation-related trigger starts the acquisition of the incoming photon events over a few oscillations period, which warrants perfect reproducibility for each pass. The channel width (the temporal resolution) is 100 ns. Hundreds of thousands of passes are necessary to obtain a good LIF signal-to-noise ratio. For each velocity group measurement, the laser wavelength is kept constant through a feedback loop. The LIF signal is extracted through two successive measurements laser on and laser off. The subtraction reveals the fluorescence events collected by the pulse counting device. The statistics is optimized when the substraction is operated after each pass.

Results

In order to validate the use of the oscillations control to perform TR-LIF, time-averaged LIF (TA-LIF) has been performed with and without the modulation. Fig. 4 shows the IVDF obtained with and without use of the modulation system. The spectra match each other at

Distribution A: Approved for public release; distribution is unlimited.

almost all velocities. One notices a slight difference on the low velocities part of the main peak. The velocity gap is however close to the measurement error. The discrepancy is likely to originate from the thruster thermal drift.

Fig. 5 represents the reconstruction of the time-averaged IVDF from the time-resolved data. The blue line is the raw TA-LIF profile obtained from the lock-in detection technique. The temporal mean of each time-varying velocity group (in red squares) perfectly match the time-averaged measurements, which validate our approach. Several positions have been examined inside and outside the discharge channel and always show a perfect agreement between time-resolved and time-averaged LIF.

The effect of the modulation upon the ions depend strongly on their velocities. Fig. 6 represents time-series for several ion groups. Recorded waveforms have been filtered by a low-pass Fourier filter with a cut-off frequency of 400 kHz, preserving all the breathing mode characteristics. Raw LIF data directly obtained from the photon counting as well as corresponding filtered data are depicted in Fig. 6.

The ion response to the excitation can be easily observed from the raw data. The lower velocity group does not seem to oscillate at all. This group is at the low velocity tail of the IVDF and represents a very few percent of the total ion population. Mean value of the LIF signal is well above zero, meaning the statistics is good enough to properly extract the fluorescence signal. On the contrary, the two other groups are oscillating. It is worth noticing that breating mode appear on filtered data as well as higher frequency ion oscillations with $f \approx 200$ kHz. These high frequency waves are likely to be associated to the so-called ion transit time oscillations. The contour map of the temporal IVDF is plotted in Fig. 7.

Conclusion

The examination of the temporal characteristics of a cross-field discharge has been performed by means of TR-LIF spectroscopy. Several results are of great interest. First, the photon-counting technique is shown to be valid as a diagnostic technique provided the discharge oscillations can be maintained in a quasi-harmonic regime. Second, we have demonstrated the possibility to actively control low frequency oscillations by means of a potential modulation on a floating electrode, without change of the plasma mean behavior. The association of both the modulation and the TR-LIF techniques appears to be very effective to obtain time-resolved measurements.

References

[1] G. Bourgeois S. Mazouffre M. Guyot A. Lejeune, K. Dannenmayer and S. Denise, Ionization and acceleration processes in a small, variable channel width, permanent-magnet Hall thruster, J. Phys. D: Appl. Physics **45**, 185203 (2012).

[2] S. Mazouffre, Laser-induced fluorescence diagnostics of the cross-field discharge of Hall thrusters, Plasma Sources Sci. Technol. **22**, 013001 (2013).

[3] D. Gawron S. Mazouffre and N. Sadeghi, A time-resolved LIF study on the ion velocity distribution function in a Hall thruster after a fast current disruption, Phys. Plasmas **16**, 043504 (2009).

Distribution A: Approved for public release; distribution is unlimited.

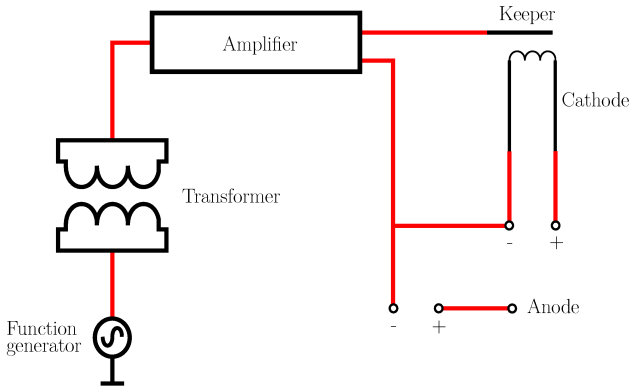

Fig. 1 : Electrical set-up of the keeper modulation.

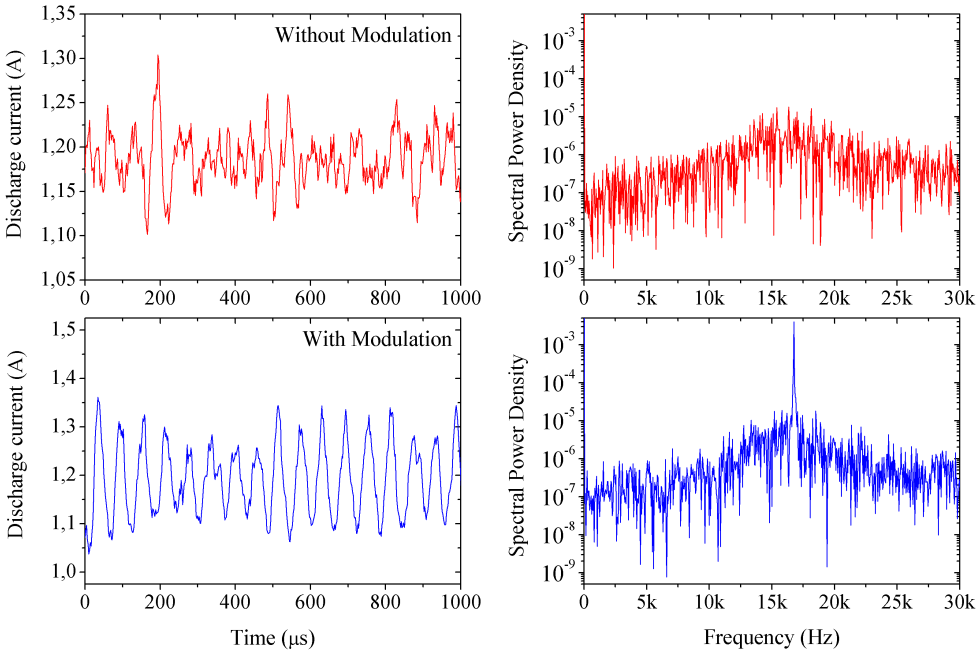

Fig. 2 : Discharge current and corresponding power spectrum with and without the keeper modulation.

Distribution A: Approved for public release; distribution is unlimited.

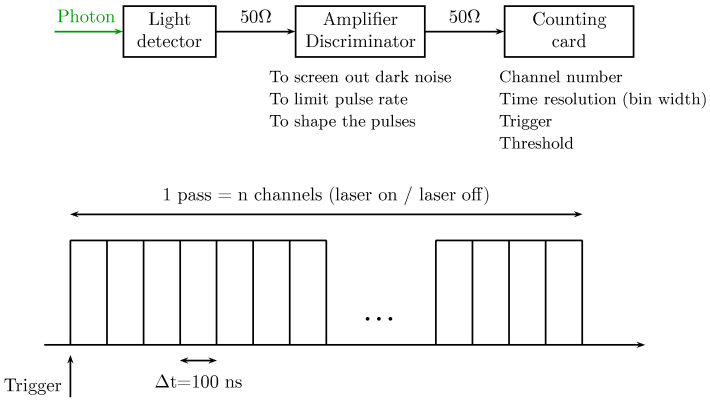

Fig. 3 : Block diagram of the detection system. Also shown is the counting card principle.

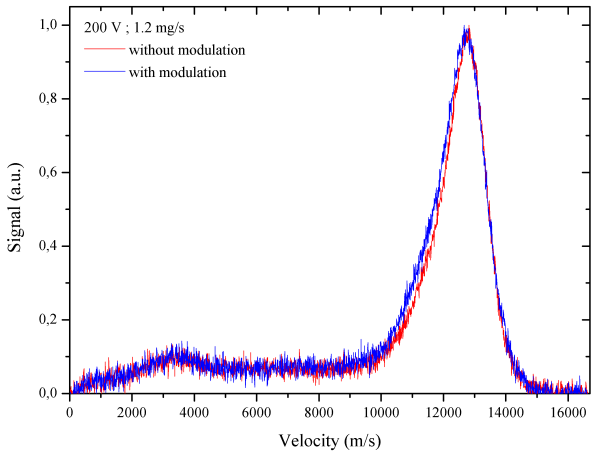

Fig. 4 : Time-averaged IVDF with and without the modulation unit.

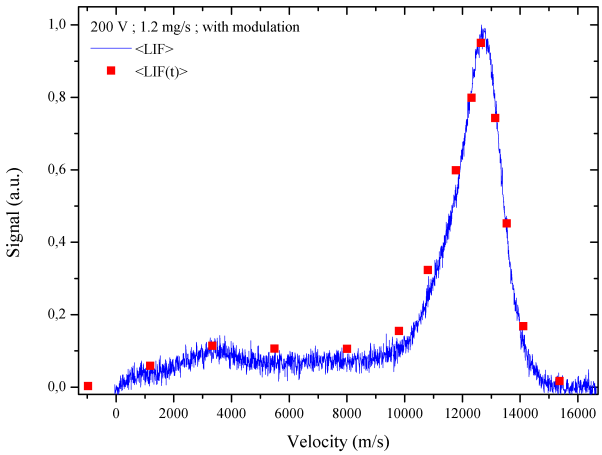

Fig. 5 : Comparison between the IVDF obtained by time-averaged measurements and the IVDF inferred from photon counting.

Distribution A: Approved for public release; distribution is unlimited.

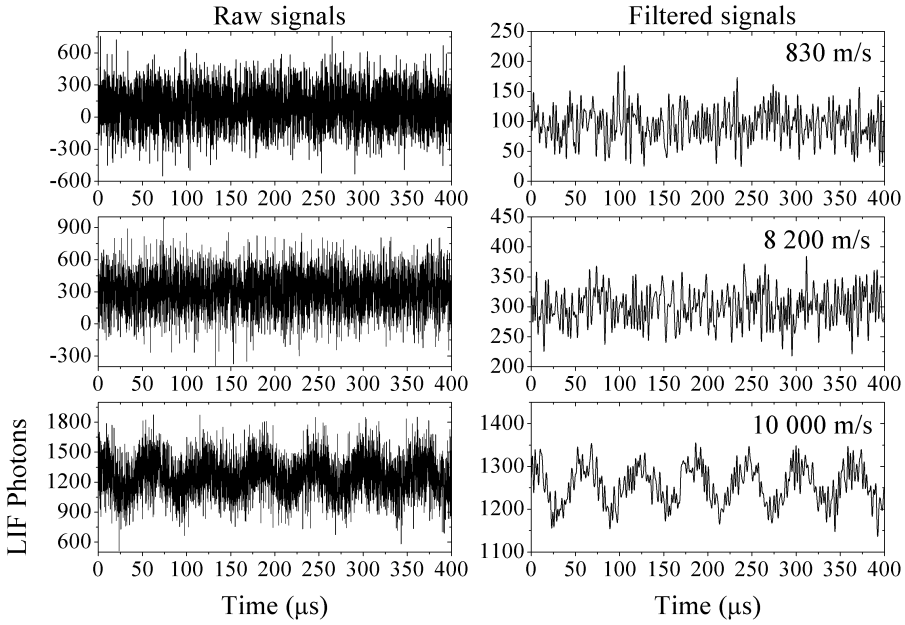

Fig. 6 : Temporal oscillations of selected velocity groups. Time series are expressed in LIF photon number against time

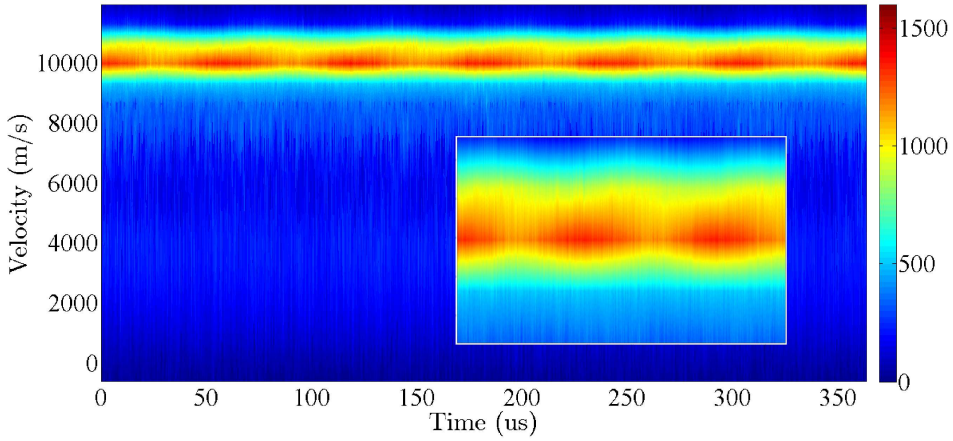

Fig. 7 : Contour plot of the temporal evolution of an IVDF over a few oscillation periods. The insert highlights the first 150 μs evolution of the most probable velocity groups. The color bar is identical for the two plots.

Distribution A: Approved for public release; distribution is unlimited.

Measurement of Perturbed Ion Velocity Distribution Function Using Time-Resolving Laser Induced Fluorescence in a Cylindrical Hall Thruster with Driven Spoke

Y. Shi, A. Diallo and Y. Raitses
PPPL, Princeton, NJ, USA

L. Balika and S. Mazouffre
CNRS - ICARE, Orléans, France

Introduction and Motivation

Hall thruster is a type of E×B discharge device used in electric propulsion. The plasma in Hall thrusters is weakly collisional with magnetized electrons and non-magnetized ions. In conventional annular geometry Hall thrusters, the applied magnetic field is mainly in the radial direction and therefore, it confines electrons in the axial direction, along which the electric field is established. The applied electric field accelerates ions producing thrust as they leave the thruster. The space charge and current of the outgoing ion flux are neutralized by additional electrons emitted from the cathode. In ideal case, the discharge is sustained by cross field diffusion of electrons, which gain enough energy to ionize the neutrals as they move towards the anode. However, in reality, two unwanted processes exist. The first process is the plasma-surface interaction in the thruster channel which causes the degradation of the thruster efficiency and limits the thruster lifetime due to the heating and erosion of the channel walls. The plasma-wall interaction can be reduced by reducing the channel surface to volume ratio, such as what has been done in a cylindrical Hall thruster (CHT) developed at PPPL [1]. In the CHT, the annular part is shrunk, creating a cylindrical channel (Fig. 1).

Another unwanted process is the anomalous transport of electrons across the magnetic field, which is typical for all types of Hall thrusters. The anomalous transport creates unnecessary current, which reduces the efficiency of the thruster and heats the electrodes. The excessive cross-field current limits the maximum achievable electric field and shifts the ion acceleration region outside the thruster channel, leading to diverged plasma plume.

There is a number of mechanisms responsible for the anomalous cross field transport, including fluctuation induced (Bohm-type) transport, near-wall conductivity induced by secondary electron emission from the wall, and transport due to plasma inhomogeneities such as coherent structures. For CHT, one of the major mechanisms of the anomalous transport is so-called rotating spoke [2]. In order to find effective ways to suppress the unwanted effects caused by anomalous transport, it is imperative to understand the mechanism responsible for the spoke. This is exactly the objective of the joint efforts by PPPL, CNRS-ICARE and University of Greifswald. In particular, we explore how spoke affects ion velocity distribution function in the CHT.

Distribution A: Approved for public release; distribution is unlimited.

Approach to Time-Resolving Measurement of Ion Velocity

Doppler Effect is used to measure ion velocity. In our experiments, xenon is used as propellant. The $5d^4F_{5/2}$-$6p^4D_{5/2}$ transition of Xe^+ is excited using tunable diode laser. Fluorescence photons from $6p^4D_{5/2}$-$6s^4P_{3/2}$ transition are collected by a photomultiplier tube and counted by a multichannel scaler (MCS). By setting laser frequency to a specific value f_s around the transition frequency ν_0, only ion with specific velocity v will observe the laser frequency to be $f_o=\nu_0$, and hence be excited. The number of ions with velocity v is thus proportional to the number of fluorescence photons when the laser frequency is set to be f_s. A picture of the optical bench is shown in Fig. 2.

To achieve time-resolving measurement at one ion velocity, laser frequency is fixed and a MCS is used to record the number of photons arrived in each one of the continuously stacked time bins. To subtract background, a mechanical chopper is used to generate laser pulses whose power is monitored by a photodiode. To increase the statistical confidence of results, accumulation of fluorescence is needed, and to achieve phase-locked accumulation of fluorescence photons, spoke is driven using successively phase-shifted square waves on anode segments where the driving signal is used to synchronize photon accumulation to spoke in data post processing. By scanning laser frequencies, the time-dependent profile of velocity distribution function can be constructed.

Preliminary Results on Driven Spoke

Affirmed by our previous success on suppressing the spoke using resistors on anode segments [4], we proposed driving spoke using square-wave voltage on segmented anode (Fig. 3), and coherently rotating azimuthal modes in CHT have indeed been successfully driven. When using resistors on anode segments, the enhanced cross field transport through spoke results in the reduced voltage on anode segment. This reduces heating of plasma inside the spoke and hence limits ionization inside the spoke, which leads to the reduction of plasma density, which causes the spoke to disappear. When driving spoke using square-wave voltage on anode segments, the exactly opposite process occurs. By applying higher voltage on one anode segment, local plasma density increases as the result of extra heating of plasma on this anode segment, and spoke appears as the consequence of this azimuthal non-uniformity. Unlike naturally occurring spoke which rotates only in ExB direction with some specific frequency, coherently rotating modes can be driven in both ExB and -ExB directions, whose frequencies exactly follow driving frequencies. To drive these modes, square-wave voltage between 225 V and 275 V is applied onto four anode segments with successive 90º phase shift. The driving circuit is operated at frequencies ranged from 50 kHz to -50 kHz, where positive and negative frequencies corresponded to rotation in ExB and -ExB direction respectively. Modes appear to be less intense but more coherent in “direct” magnetic configuration compared with “cusp”; and for each magnetic configuration, the degree of coherence shows strong dependence on driving frequency. Driving at frequencies deviate from the spoke frequency suppress the naturally occurring azimuthal mode, while driving at spoke frequency enhance the coherence of natural spoke. This resonant behavior is observed by a fast camera as well as current through anode segments.

Distribution A: Approved for public release; distribution is unlimited.

Two sequences of color-added fast camera images are shown in Fig. 4 for driving at 10 KHz (top) and -10 KHz (bottom) in cusp magnetic configuration. Image sequences for other driving frequencies are similar except for different degree of coherence. Image sequences for "direct" configuration appear to be more coherent but less intense. The frequency of a driven azimuthal mode is exactly the same as driving frequency, as can be seen in Fig. 5. The average brightness on a segment is calculated by averaging over all the pixels covering the segment, and the FFT is applied on the brightness time series for each driving frequency. Islands in Fig. 5 correspond to peaks in FFT spectrum of a number of driving frequencies.

For random fluctuation in the discharge, the brightness time series of two anode segments should be uncorrelated, whereas for ideally rotating spoke, two such brightness time series should be identical up to some phase shift, in which case, the correlation between two phase shifted time series is one. More generally, the degree of coherence of the mode driven at frequency f could be measured by the maximum lag-correlation between the brightness time series on two anode segments:

$$C(f) = \max_{\Delta t} corr\big(B_1(f,t), B_2(f,t+\Delta t)\big)$$

The dependence of coherence on driving frequency is shown in Fig. 6 (left). As can be seen from the figure, coherence is enhanced by driving at spoke frequency regardless of driving direction. Another aspect of the mode driven at frequency f is its intensity, which can be measured by the correlation between brightness and current time series on the same segment, normalized by the standard deviation of current:

$$I(f) = \max_{\Delta t} corr\big(B_1(f,t), I_1(f,t+\Delta t)\big)/\sigma(I_1)$$

This is equivalent to wavelet transformation of brightness time series using current trace as wavelet basis. This extracts the amplitude of brightness oscillation induced by driving. As can be seen in Fig. 6 (right), resonant features persist after eliminating heating effect by normalizing the brightness with segment current. Thus, azimuthal modes observed by camera are not just the result of azimuthally rotating axial heating. Indeed, as in spoke, these azimuthal modes involve redistribution and localization of discharge.

Preliminary Results on Time-Resolving Measurement of Ion Velocity

As preliminary result, we have measured axial ion velocity along the thruster geometric axis. Even so, ion distribution function shows oscillation with spoke. As shown in Fig. 7, fluorescence photon counts shows oscillation at period ~66.6 μs, this exactly matches the frequency of spoke, which is driven at 15 KHz in the experiment. By scanning six different laser frequencies, the time-dependent profile of ion velocity distribution function has been reconstructed, as has been shown in Fig. 8 (left). The averaged distribution functions at spoke maximum and spoke minimum are shown in Fig. 9 (left). The error bars for "With Spoke" and "Without Spoke" are the standard deviations of the spoke maxima and minima counts, respectively. For example, error bar of photon counts for ions at velocity 13.3 Km/s in case "With Spoke" is the standard deviation of the four peak values in Fig. 7. As can be seen in Fig.

Distribution A: Approved for public release; distribution is unlimited.

9 (left), along the thruster axis, ion density is strongly modulated. On the other hand, as shown in Fig. 9 (right), the fact that the normalized velocity distribution functions overlap up to error bars indicates that axial ion velocities are not substantially affected.

Heterodyne LIF technique

As previously explained, to understand the fundamental mechanism at play in the spoke, we apply an external perturbation of the same spatial structure and in phase with the intrinsic spoke and probe the full ion velocity distribution function $f(v) = f_0 + f_1$, where f_0 is the equilibrium ion distribution, and f_1 is the wave-induced perturbation of the distribution. The time-varying distribution function is then obtained using the laser-induced fluorescence (LIF) diagnostic in pulse-counting mode.

We, however, discovered another approach that seems promising as it brings new opportunities in investigating the rotating spokes. It appears that a heterodyne LIF method allows to resolve simultaneously f_0 and the perturbed velocity distribution function f_1. This approach consists of driving the spoke with frequency ω_{drive}, and of modulating the laser at frequency ω_0. We then collect the LIF data with the photon-counting card for each velocity class which contains modulations of the signal at ω_0, ω_{drive}, and their sum and difference. The amplitude of LIF signal at ω_0 for each velocity class yields the equilibrium (unperturbed) ion velocity distribution, while the amplitude of the LIF signal at $\omega_0 \pm \omega_{drive}$ yields the wave-phase coherent induced perturbed distribution. In this project we have demonstrated the proof-of-principle of this technique. Figure 9 is the power density spectrum (Fourier spectrum) of a fluorescence time-series for a given ion velocity group with modulation voltage. The presence of two peaks at the sum and difference frequency indicates the ion group oscillates at the spoke frequency. Futher studies will be aimed at fine-tuning this approach for determining the wave-induced perturbation from which a dispersion relation of the spoke instability can be experimentally determined.

Distribution A: Approved for public release; distribution is unlimited.

References

[1] Y. Raitses and N. J. Fisch, Physics of Plasmas, **8**, 2579 (2001). A. Smirnov, Y. Raitses, and N.J. Fisch, Physics of Plasmas **14**, 057106 (2007).

[2] J. B. Parker, Y. Raitses, and N. J. Fisch, Applied Physics Letters **97**, 091501 (2010).

[3] C. L. Ellison, Y. Raitses and N. J. Fisch, Physics of Plasmas **19**, 013503 (2012)

[4] M. E. Griswold, C. L. Ellison, Y. Raitses, and N. J. Fisch, Physics of Plasmas **19**, 053506 (2012).

Distribution A: Approved for public release; distribution is unlimited.

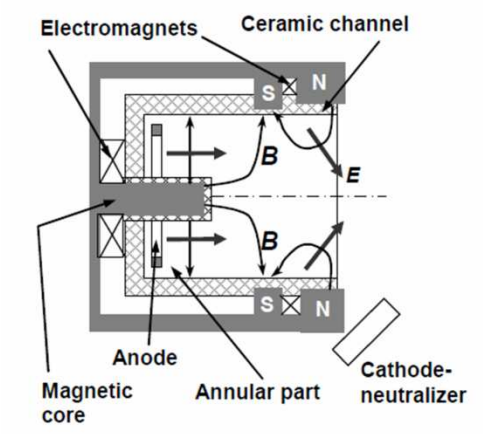

Fig. 1: Schematic of CHT

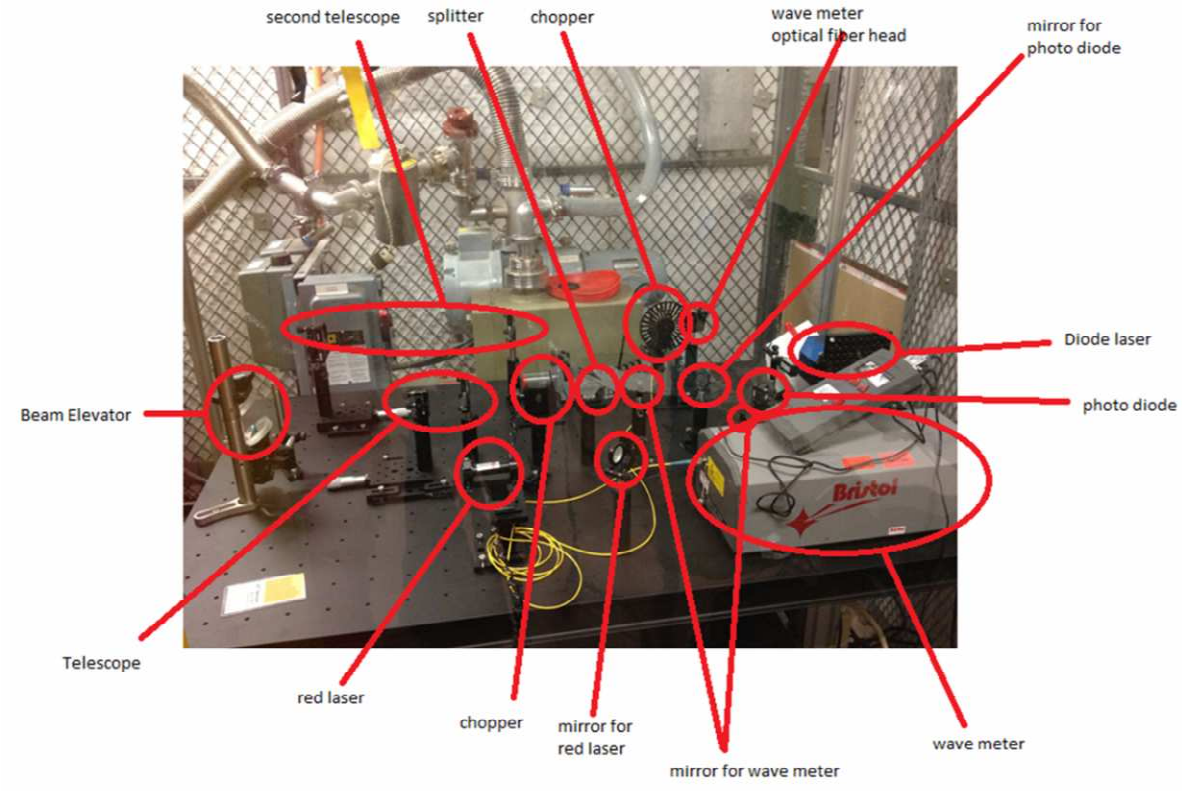

Fig. 2: Optical table of the LIF setup

Distribution A: Approved for public release; distribution is unlimited.

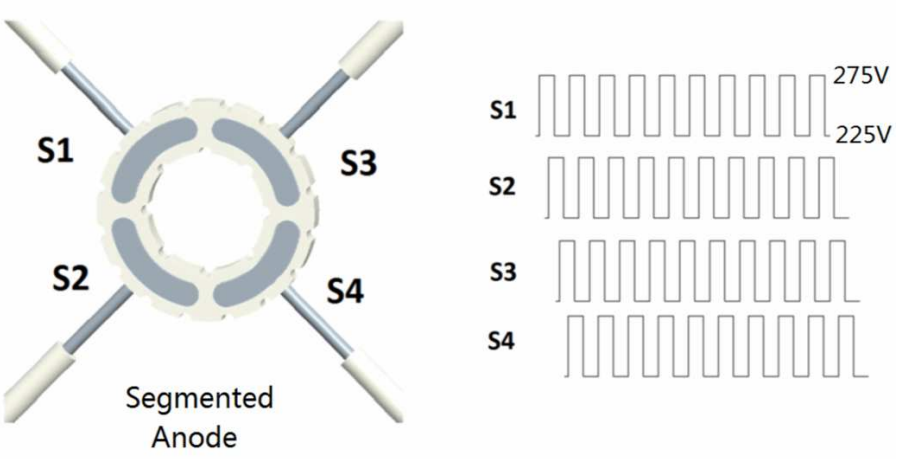

Fig. 3: Schematic of driving spoke using segmented Anode

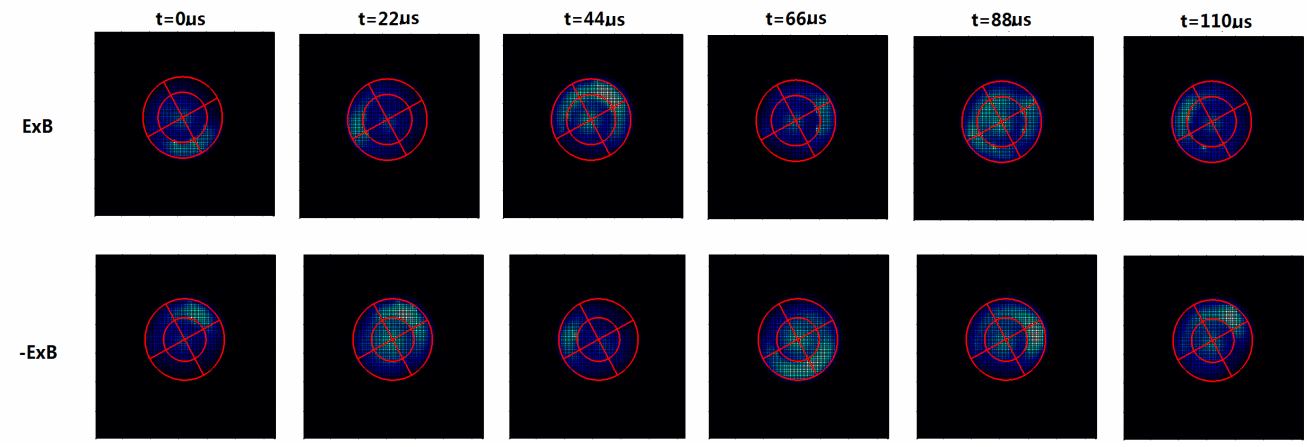

Fig. 4: Sequence of fast camera images (color added) for driving at 10 KHz (top) and -10 KHz (bottom). The magnetic field was in "cusp" configuration. The inner red circle encloses the magnetic core and outer red circle shows the location of thruster channel. The boundaries of four anode segments are also shown.

Distribution A: Approved for public release; distribution is unlimited.

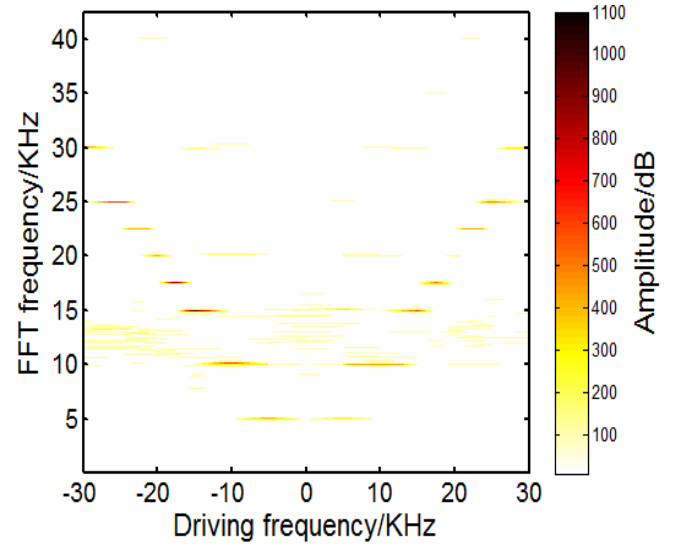

Fig. 5: Fourier spectra of segment brightness. Each island corresponds to one driving frequency.

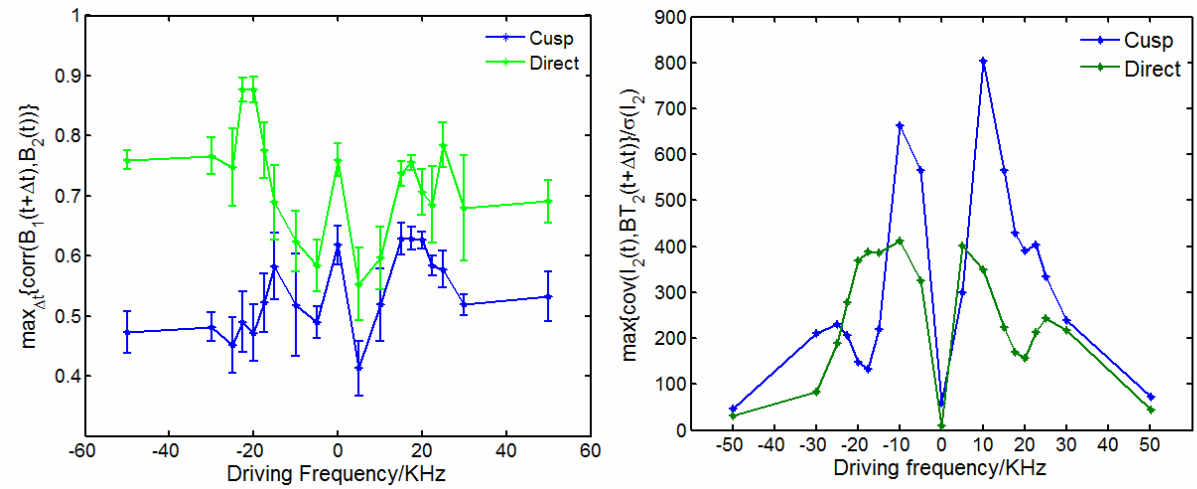

Fig. 6: Mode coherence as measured by maximum lag-correlation of brightness time series on two anode segments (left). Mode intensity as measured by maximum lag-covariance of brightness and current time series normalized by current amplitude (right).

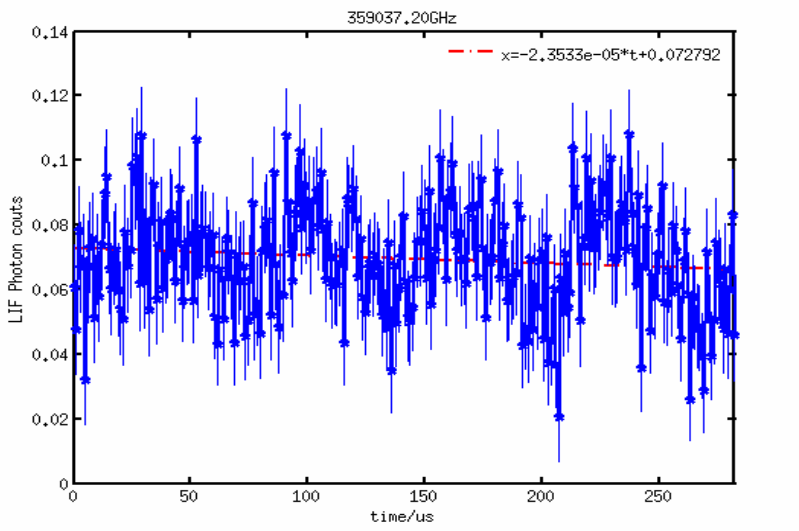

Fig. 7: Time series of fluorescence photon counts at laser frequency 359037.20 GHz. The vertical bars show the estimated errors.

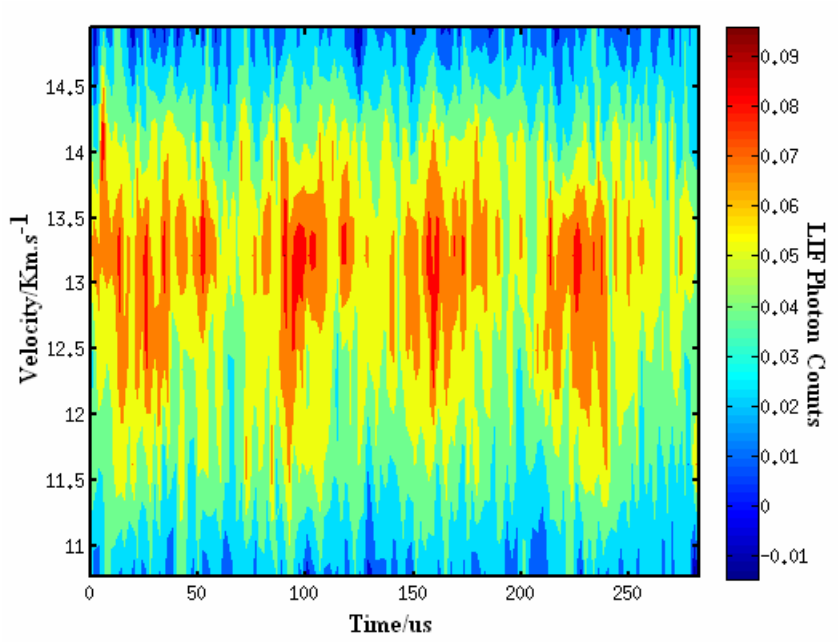

Fig. 8: Contour plot of time-dependent ion velocity distribution function profile

Distribution A: Approved for public release; distribution is unlimited.

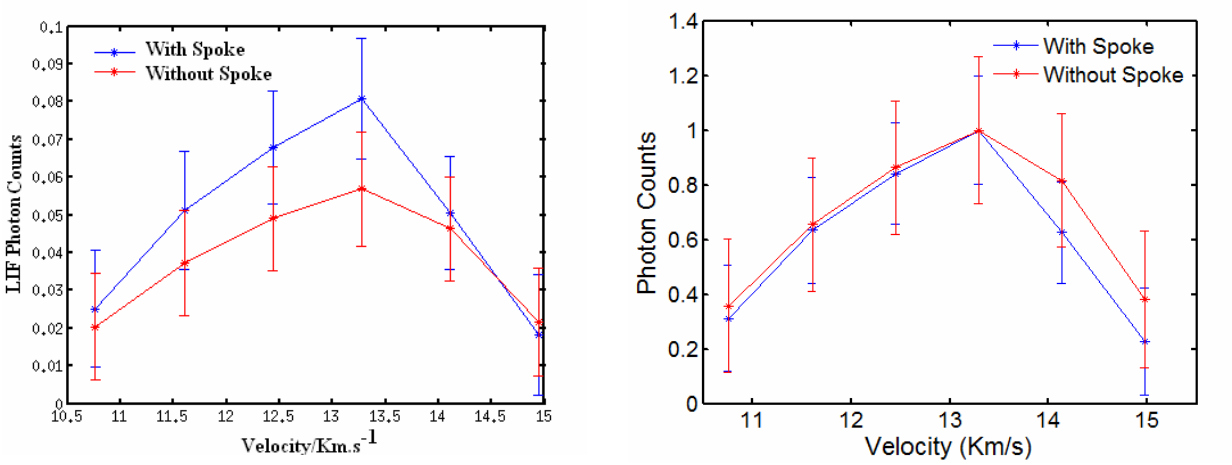

Fig. 9: Ion velocity distribution function with/without spoke (left). Normalized ion velocity distribution functions (right).

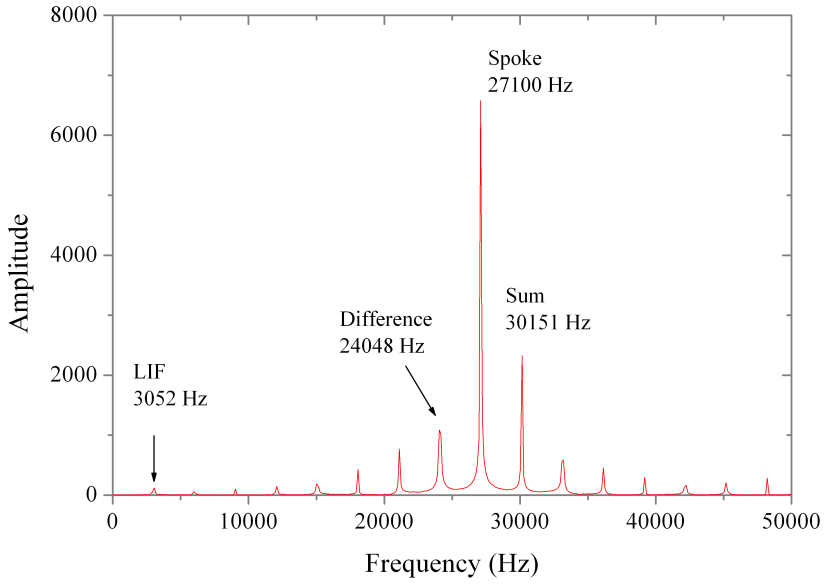

Fig. 10: Outcome of the heterodyne LIF measurement: Power spectrum density (Fourier space) of an ion velocity group time-series showing the expected modes.

Distribution A: Approved for public release; distribution is unlimited.

Numerical simulations of CHT thruster

R. Schneider and K. Matyash
EMAU, Greifswald, Germany

Introduction

Within the project the self-consistent 3D-3V Particle-in-Cell simulation code STOIC [1] was extended with a diagnostic module for monitoring the 3D ion flow pattern in the CHT thruster.

Sensitivity studies were performed where the influence of computational particles statistical weight on the simulation results was investigated. The studies have shown that at least 5×10^7 computational particles are necessary to ensure the accurate simulation of the CHT thruster.

The spoke and non-spoke regimes of the CHT operation were achieved in the simulations (Fig. 1). In agreement with the experiment [2], the transition from spoke to non- spoke regime was observed in the simulations with an increase of the electron current from the cathode.

Impact of the rotating spoke

In order to investigate the effect of the spoke on the ion flow in the thruster, the ion flow velocity was averaged over 5 cycles of the spoke rotation. The averaged ion velocity vector map at the longitudinal axial cross-section of the simulation domain for spoke and non-spoke regimes is presented in Fig. 2. As one can see from the simulation, in the spoke regime ion velocity in the thruster channel is distinctly lower as compared with the non-spoke regime. Furthermore, in the spoke regime the simulated ion flow velocity outside of the thruster, away from centerline, exhibits visibly higher divergence as compared with the non-spoke cathode overrun regime. This agrees well with experimental measurements in [3]. It is difficult to distinguish the quantitative differences between the spoke and non-spoke regimes in the vector maps. For quantitative analyses the color maps of the total ion velocity and the three velocity components with and without spoke are presented separately in Figs 3-6. Here one can see that in the spoke regime the largest part of the ion acceleration takes place outside of the thruster, in the plume. In contrast, without the spoke the largest part of acceleration happens inside the thruster. The maximum exhaust ion axial velocity in both cases is about 16 km/s. The axial ion velocity at the thruster exit is 5.4 km/s with the spoke and 9.2 km/s without spoke. This agrees quite good with findings in [3] and the experimental observations within the current project.

Ion velocity

Analyzing the azimuthal component of the ion velocity, one can see that in both spoke and non-spoke cases its magnitude reaches the maximum of about 0.2 km/s in the region where the magnetic field is strongest - close to the thruster annular channel. Here, the azimuthal velocity component is comparable with the total ion velocity. The local magnetic field is strong enough to notably bend the ion trajectories before ions can leave this region. In the rest

Distribution A: Approved for public release; distribution is unlimited.

of the computational domain the azimuthal component of the ion velocity in both spoke and non-spoke cases is much smaller than the total ion velocity. Outside the thruster the maximum ratio of the azimuthal and total velocity is about 2 %. This corresponds to the tilt of the velocity flow of about 1 degree.

Stronger ion acceleration inside the thruster channel in the non-spoke regime points out at the larger potential drop inside the channel as compared to the spoke regime. In Fig. 7 the plasma potential map for both regimes is presented. Indeed, in the non-spoke case the potential drop inside the thruster is 140 V, whereas with the spoke it is only 40 V. These results are in agreement with former experiments [4]. Such difference in potential can be only explained by increased plasma conductivity in the spoke regime. As the plasma density in both cases is approximately equal, see Fig. 8, the higher plasma conductivity can only be caused by the presence of the additional transport mechanism - perpendicular electron transport caused by the spoke [5].

Flow asymmetry

In order to see the dynamics of the ion flow due to the spoke rotation, the averaging time in the simulations was reduced by factor of 100, such that the spoke rotation cycle was resolved. Reduction of the averaging time led to an increase of the statistical noise in the simulation results. However, the effect of the rotating spoke on the ion flow could be unambiguously identified. In the figures 9-12 the plasma parameters at four phases of the spoke rotation cycle are presented. The spoke position can be identified at the transverse cut of the ion density inside the annular channel (Figs. 9d, 10d, 11d, 12d). The rotating inhomogeneity of the plasma density leads to the rotating asymmetry in the electric potential (Figs. 9f, 10f, 11f, 12f). The potential profile defines the ion flow in the thruster. The rotating asymmetry of the potential leads to the rotating asymmetry of the ion velocity. The fluctuations up to about 13% are visible in the axial velocity at the thruster exit (Figs. 9b, 10b, 11b, 12b). The maximum of the axial velocity fluctuations is located at the periphery, at the radial position corresponding to the thruster radius, but at the axis fluctuations of about 4% are still observable. More clearly velocity fluctuations are visible in the azimuthal velocity plots (Figs. 9c, 10c, 11c, 12c). The azimuthal velocity at the thruster exit oscillates with the amplitude of 1.4 km/s, which corresponds to about 15% of the average axial velocity at this position. The rotating asymmetry in the ion velocity can be clearly observed in the vector map of the perpendicular velocity at a transverse cut at the thruster exit (Figs. 9a, 10a, 11a, 12a).

Conclusions

The simulations results fully support our hypothesis about the rotating spoke causing the rotating asymmetry in the ion flow in the CHT thruster. To our knowledge these are the first self-consistent simulations revealing the ion flow asymmetry caused by the rotating spoke in the plasma thruster.

In order to obtain better quantitative results, which could be compared with the experiment, better statistics in the simulation are necessary. Such improved statistics can be achieved by

Distribution A: Approved for public release; distribution is unlimited.

summing up the output for the same phase during many spoke rotation cycles. In order to be able to do that, spoke rotation in the simulation has to be coherent. Such coherent rotation of the spoke in the simulation can be achieved by applying a modulated voltage to the segmented anode, the same way as it was done in the experimental part of the project.

References

[1] K. Matyash, R. Schneider, O. Kalentev, Y. Raitses, N. J. Fisch, Numerical investigations of a cylindrical Hall thruster, IEPC-2011-070, the 32nd International Electric Propulsion Conference, Wiesbaden, Germany, September 11 - 15, 2011.

[2] J. B. Parker, Y. Raitses, and N. J. Fisch, Applied Physics Letters 97, 091501 (2010).

[3] R. Spektor, K. D. Diamant, E. J. Beiting, Y. Raitses, and N. J. Fisch, Laser induced fluorescence measurements of the cylindrical Hall thruster plume, Physics of Plasmas 17, 093502 (2010).

[4] Y. Raitses, A. Smirnov, and N. J. Fisch, Effects of enhanced cathode electron emission on Hall thruster operation, Physics of Plasmas 16, 057106 (2009).

[5] C. L. Ellison, Y. Raitses and N. J. Fisch, Physics of Plasmas 19, 013503 (2012).

Distribution A: Approved for public release; distribution is unlimited.

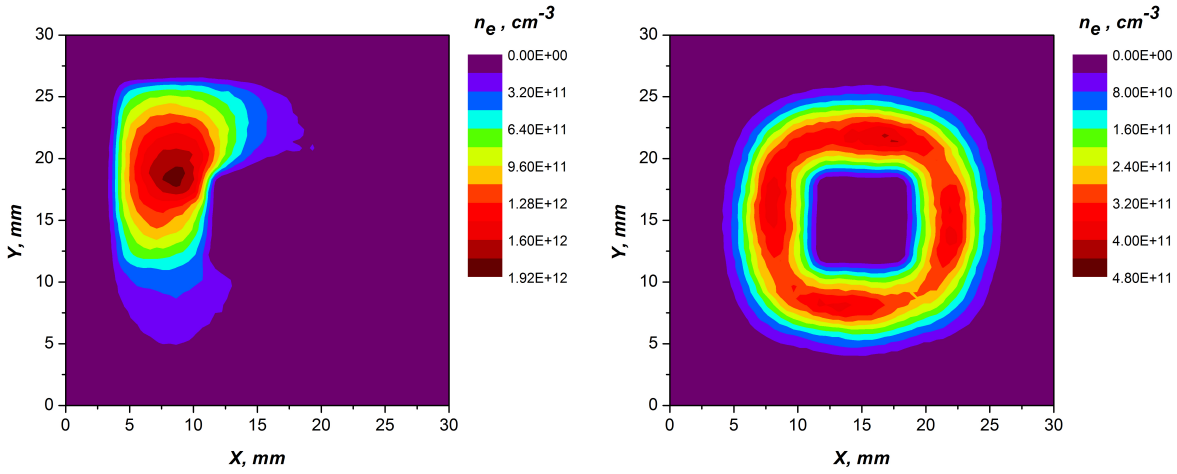

Fig. 1: Electron density in the annular channel of CHT thruster: a) spoke regime ($I_{cath} = 0.25$ A); b) non-spoke regime ($I_{cath} = 0.5$ A).

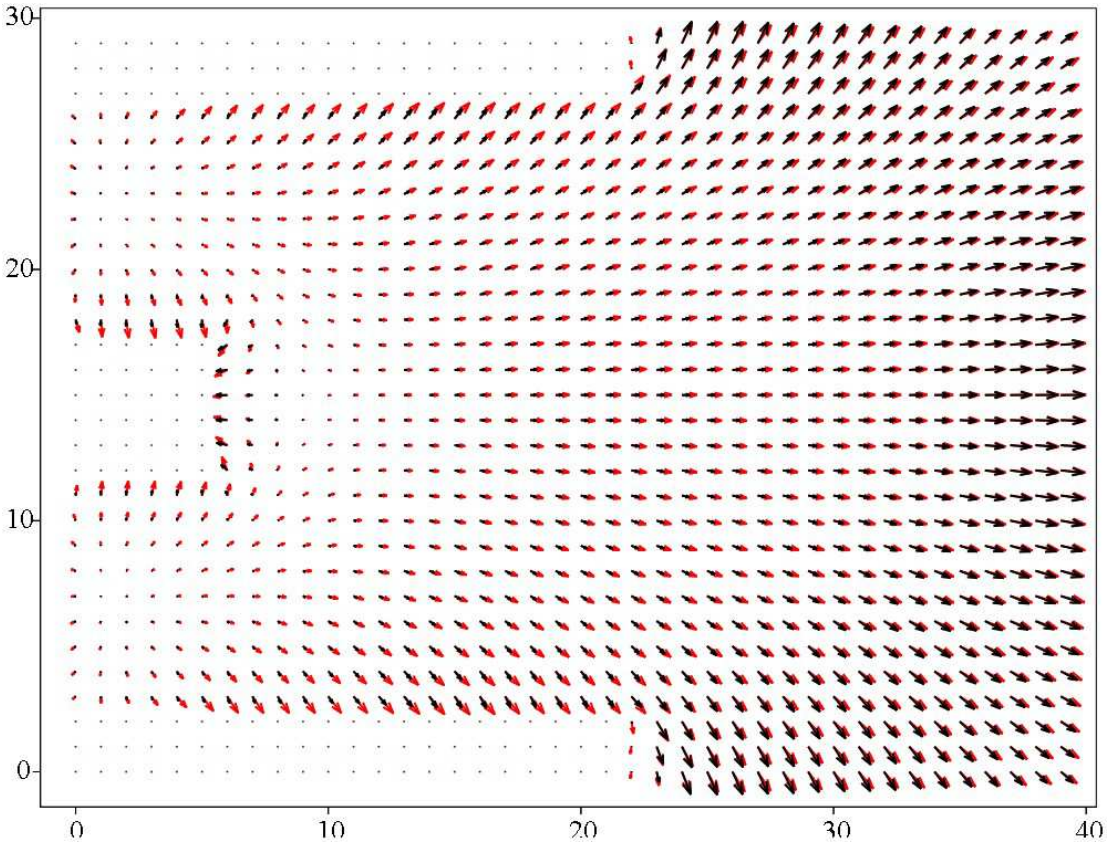

Fig. 2: Averaged ion flow map for spoke (black) and non spoke regimes (red).

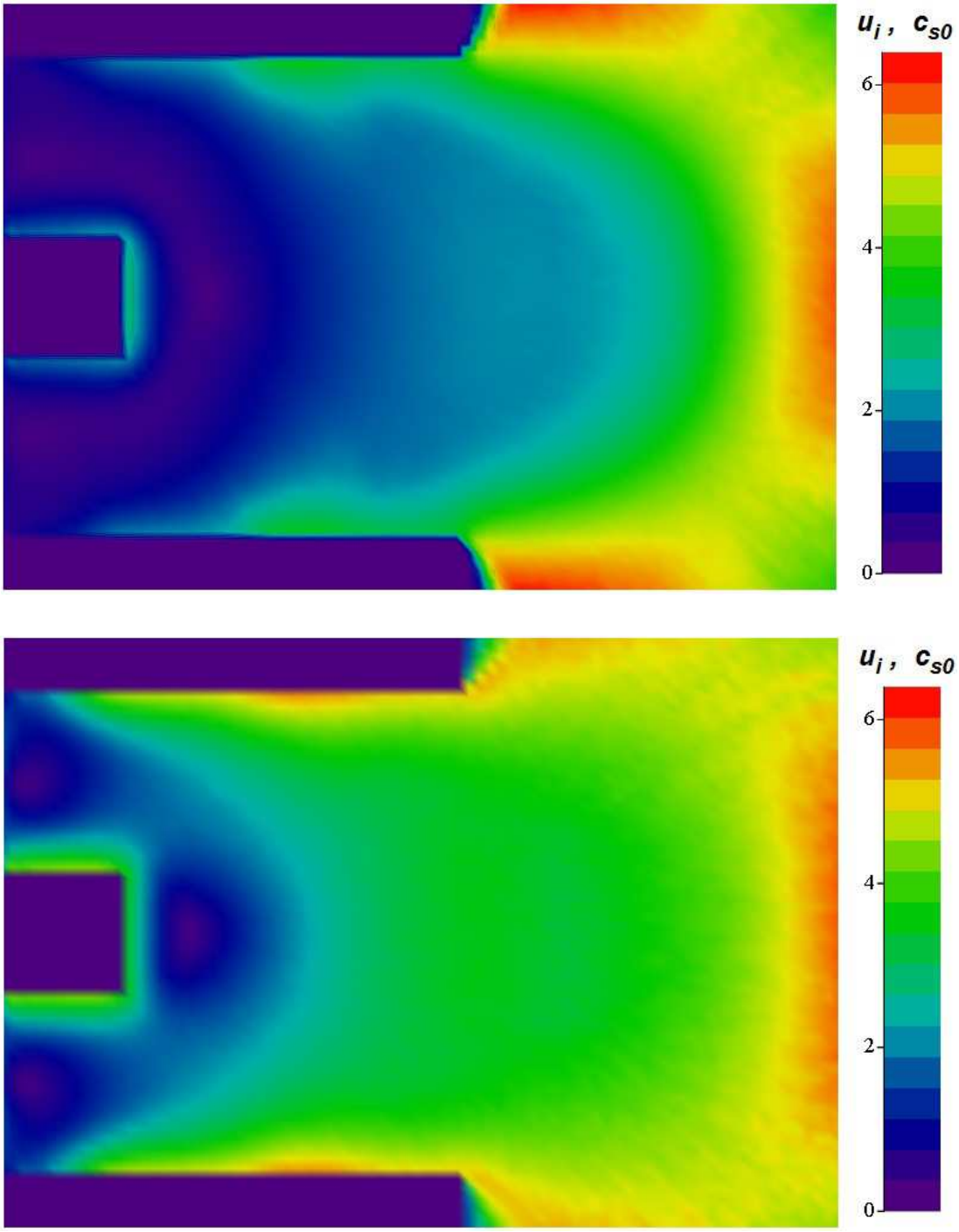

Fig. 3: Map of the total ion velocity. Spoke (top) and non-spoke regime (bottom). c_{s0} = 2.7 km/s.

Distribution A: Approved for public release; distribution is unlimited.

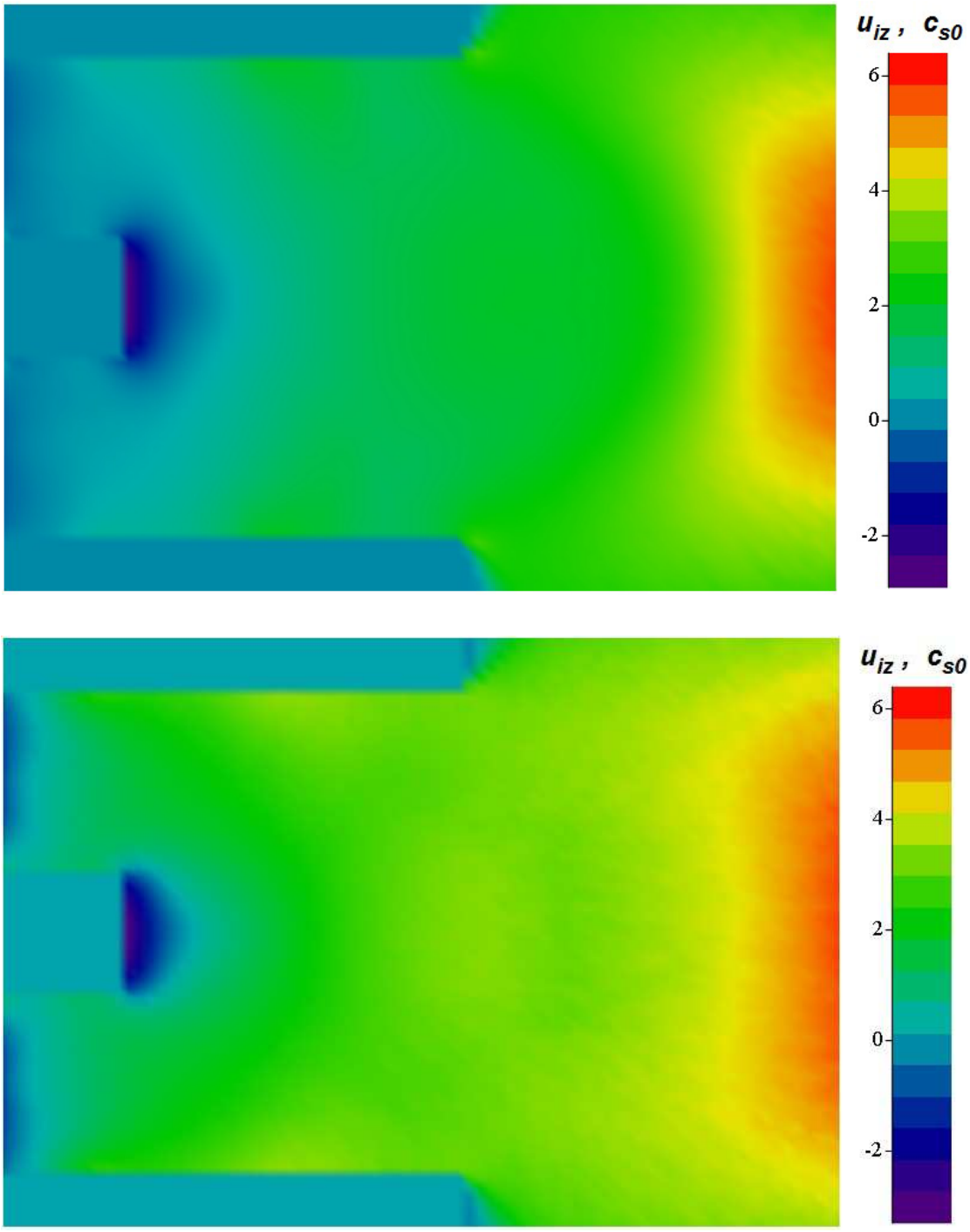

Fig. 4: Map of the axial component of ion velocity. Spoke (top) and non-spoke regime (bottom). c_{s0} = 2.7 km/s.

Distribution A: Approved for public release; distribution is unlimited.

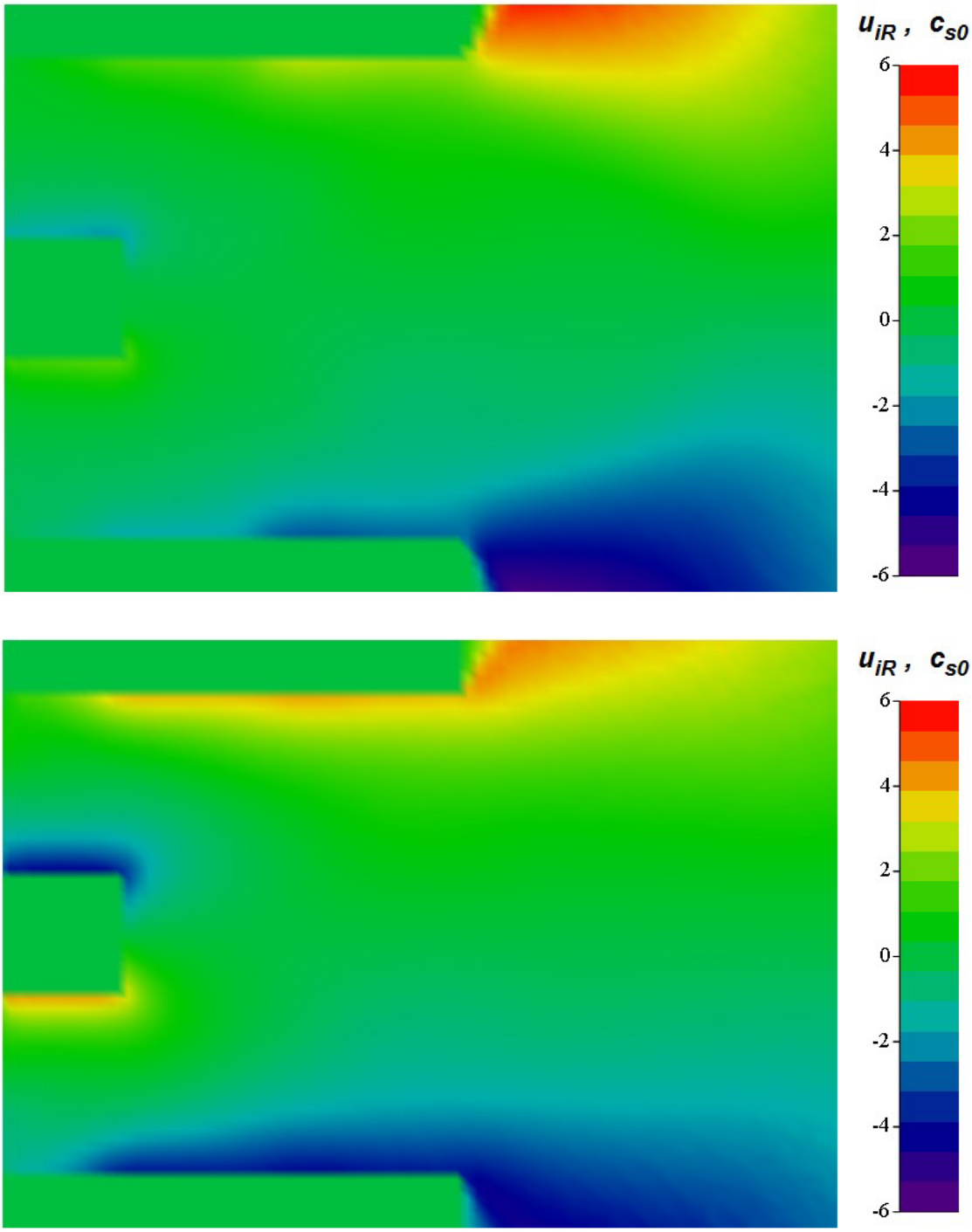

Fig. 5: Map of the radial component of ion velocity. Spoke (top) and non-spoke regime (bottom). c_{s0} = 2.7 km/s.

Distribution A: Approved for public release; distribution is unlimited.

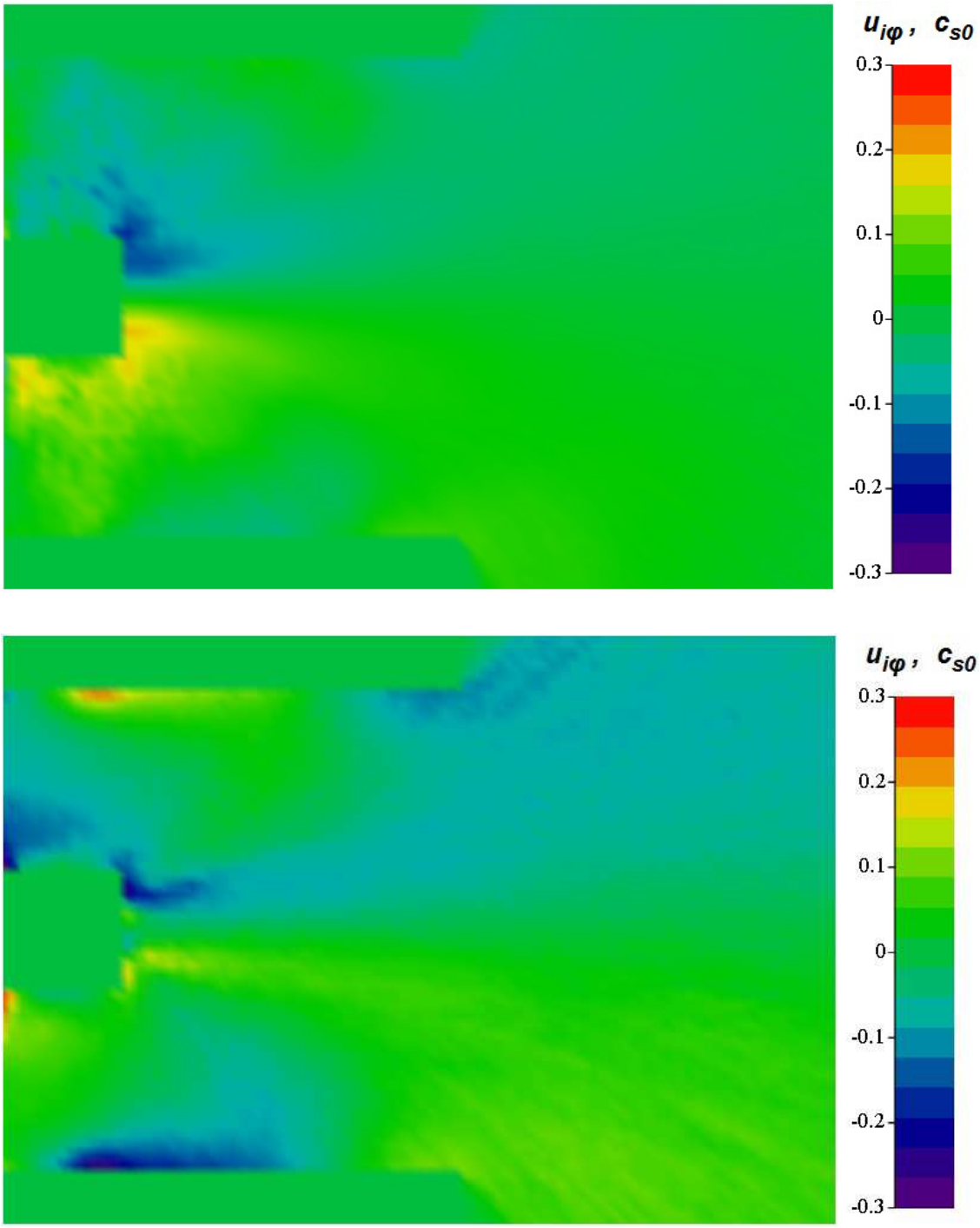

Fig. 6: Map of the azimuthal component of ion velocity. Spoke (top) and non-spoke regime (bottom). c_{s0} = 2.7 km/s.

Distribution A: Approved for public release; distribution is unlimited.

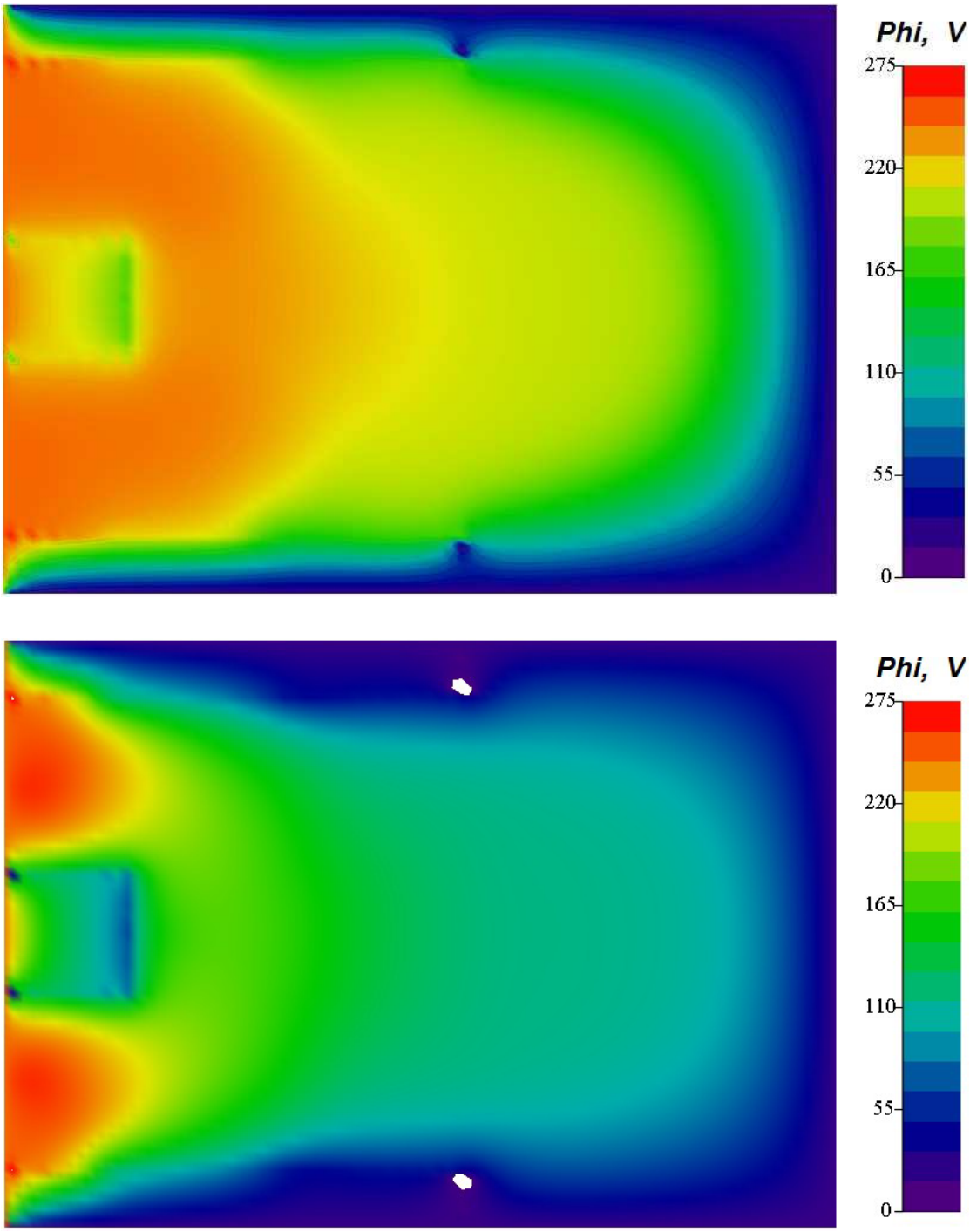

Fig. 7: Map of the plasma potential. Spoke (top) and non-spoke regime (bottom).

Distribution A: Approved for public release; distribution is unlimited.

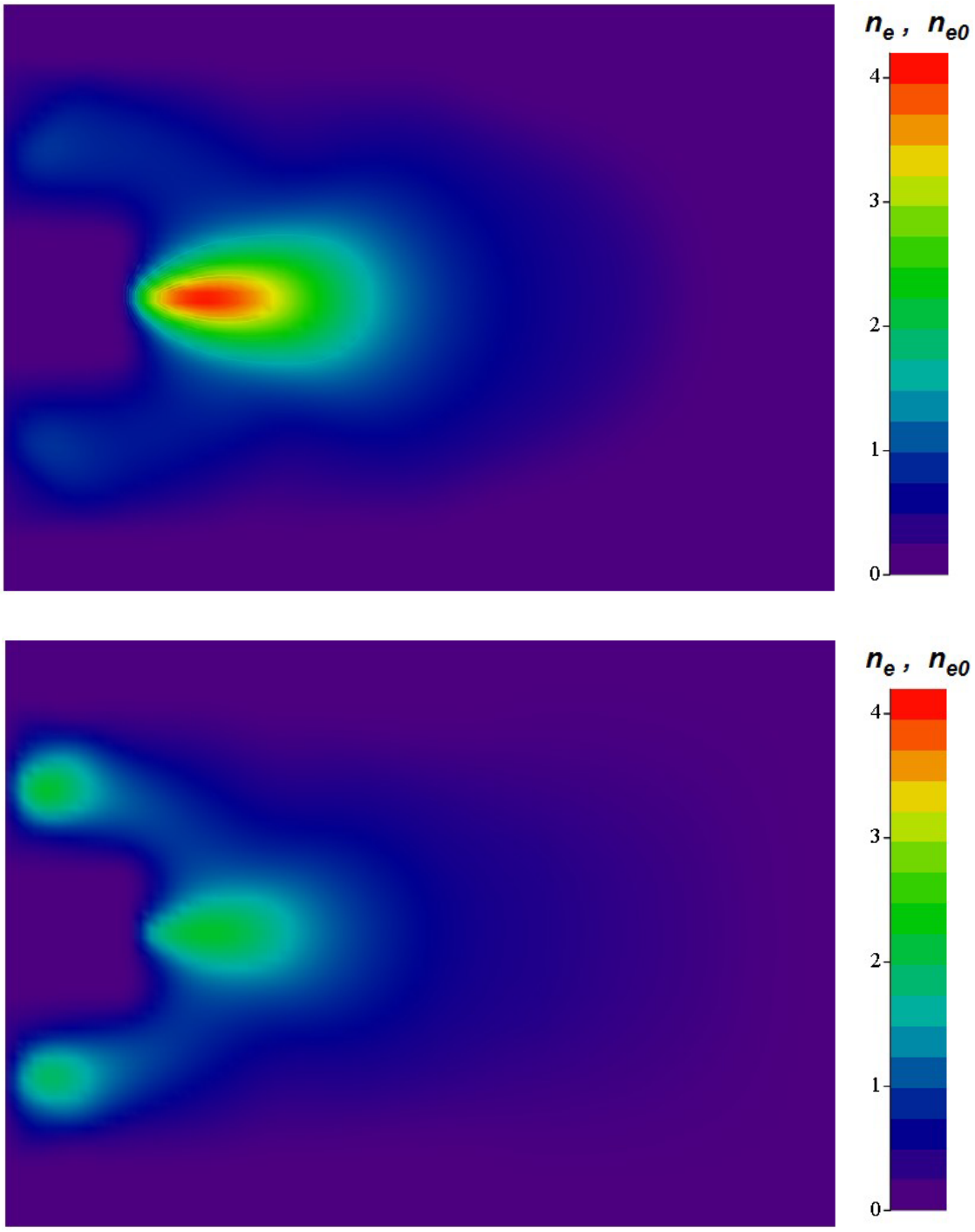

Fig. 8: Averaged map of the electron density. Spoke (top) and non-spoke regime (bottom). $n_{e0} = 4\times10^{11}$ cm^{-3}.

Distribution A: Approved for public release; distribution is unlimited.

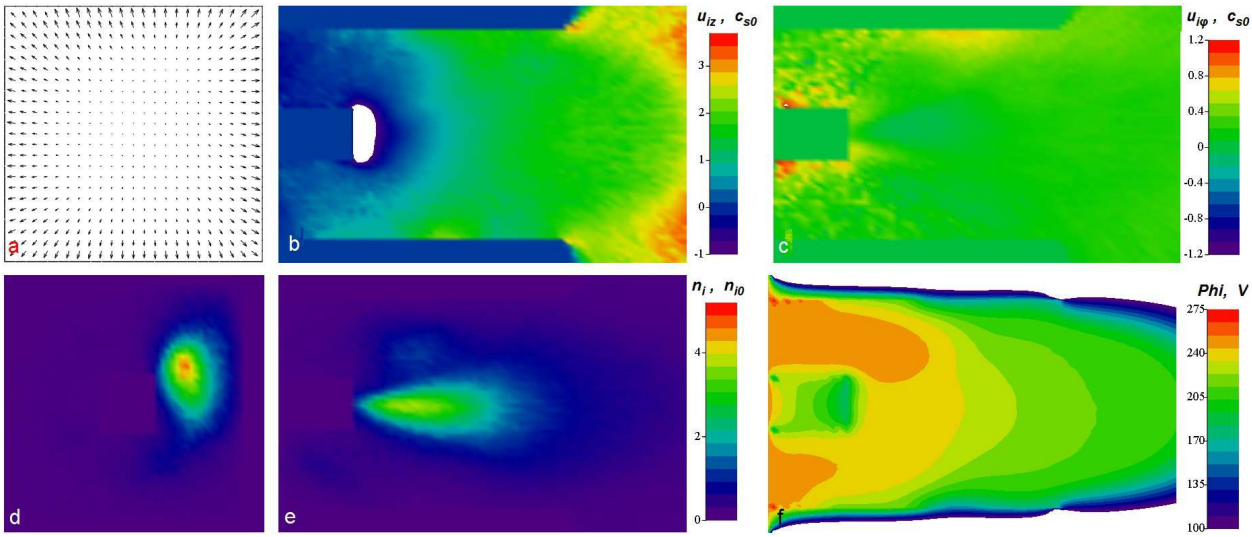

Fig. 9: Vector map of the perpendicular ion velocity at transverse cut at the thruster exit (a). Ion axial velocity (b) and ion azimuthal velocity (c) at the longitudinal axial cut. Ion density at transverse cut at the annular channel (d) and at the longitudinal axial cut (e). Plasma potential at the longitudinal axial cut. All parameters are taken at phase $\varphi = 0$.

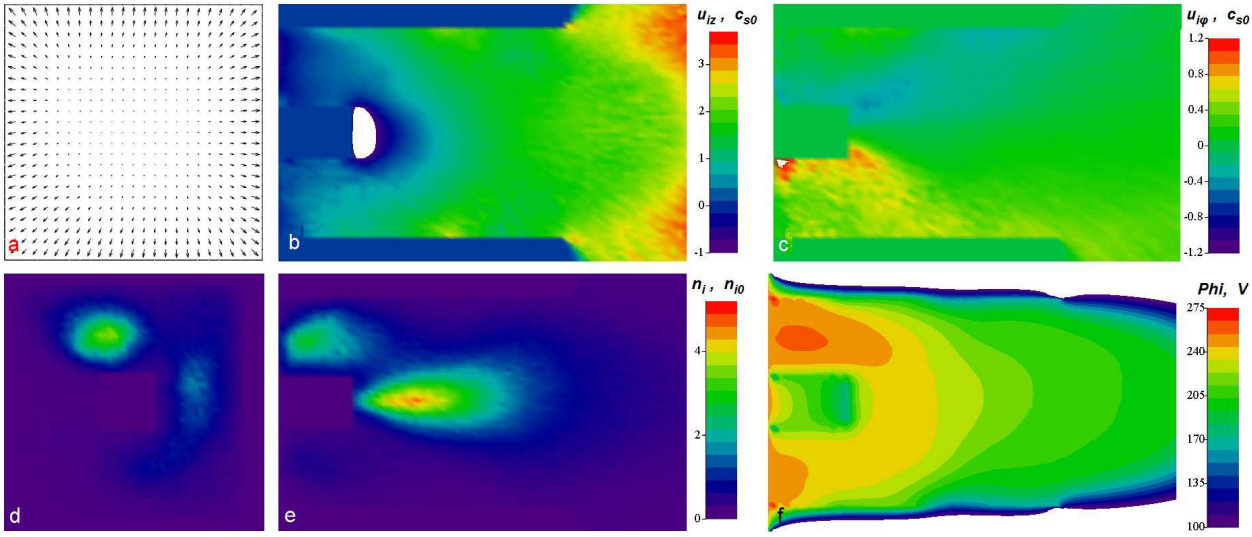

Fig. 10: Vector map of the perpendicular ion velocity at transverse cut at the thruster exit (a). Ion axial velocity (b) and ion azimuthal velocity (c) at the longitudinal axial cut. Ion density at transverse cut at the annular channel (d) and at the longitudinal axial cut (e). Plasma potential at the longitudinal axial cut. All parameters are taken at phase $\varphi = \frac{\pi}{2}$.

Distribution A: Approved for public release; distribution is unlimited.

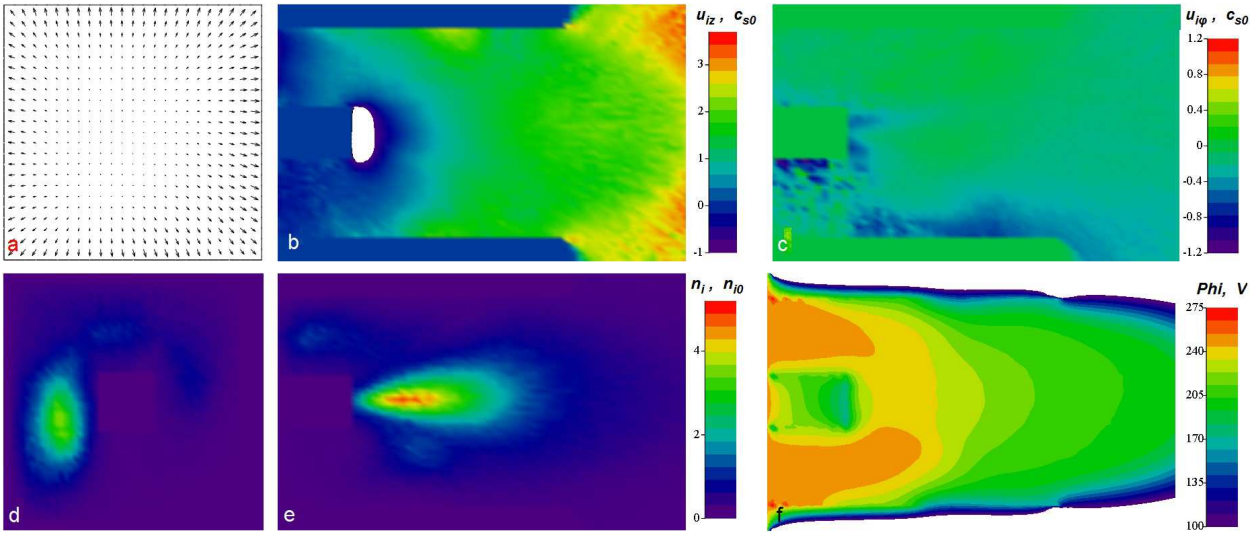

Fig. 11: Vector map of the perpendicular ion velocity at transverse cut at the thruster exit (a). Ion axial velocity (b) and ion azimuthal velocity (c) at the longitudinal axial cut. Ion density at transverse cut at the annular channel (d) and at the longitudinal axial cut (e). Plasma potential at the longitudinal axial cut. All parameters are taken at phase $\varphi = \pi$.

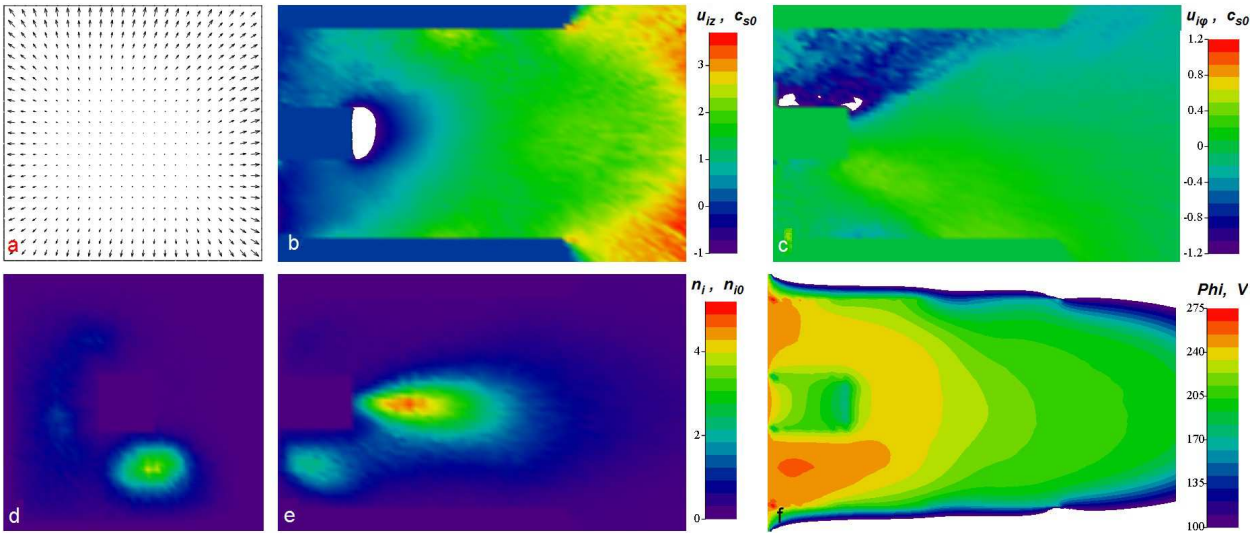

Fig. 12: Vector map of the perpendicular ion velocity at transverse cut at the thruster exit (a). Ion axial velocity (b) and ion azimuthal velocity (c) at the longitudinal axial cut. Ion density at transverse cut at the annular channel (d) and at the longitudinal axial cut (e). Plasma potential at the longitudinal axial cut. All parameters are taken at phase $\varphi = \frac{3\pi}{2}$.

Distribution A: Approved for public release; distribution is unlimited.